AIAA SciTech Forum
9 - 13 January 2017, Grapevine, Texas
55th AIAA Aerospace Sciences Meeting

10.2514/6.2017-0015

Robust design of small-scaled unmanned helicopter for hover performance using Taguchi method

D. R. Abhiram[1], Ranjan Ganguli[2], Dineshkumar Harursampath[3]
Indian Institute of Science, Bangalore, Karnataka, India, 560 012.

Peretz P. Friedmann[4]
The University of Michigan, Ann Arbor, MI, U.S.A., 48109 – 2140

A simple approach for robust design of a small-scale unmanned helicopter main rotor using Taguchi method is presented. Multiple parameters of the main rotor, viz. blade length, blade planform variation, blade pre-twist and rotor speed, are considered, with the objective of improving the hover performance of the helicopter. Each design parameter value is considered at three distinct levels. A numerical scheme based on blade element momentum theory is used for performance analysis of the helicopter. The Taguchi method is used to obtain the optimal combination of design parameter values that result in a helicopter design with improved hover performance. Robustness of the design is facilitated by using practical tolerance values of the design variables as noise factors. Analysis of variance (ANOVA) is conducted to determine the relative statistical significance of design parameters considered. Taguchi method is further used for obtaining optimal tolerance values of the design variables that lead to reduced variation in hover performance of the helicopter within a reasonable cost of quality control. The resulting robust design shows improved hover efficiency of the helicopter, with minimum variability in its performance in presence of reasonable variations in design variables.

[1] Graduate Student, Department of Aerospace Engineering; email: abhiram@aero.iisc.ernet.in
[2] Professor, Department of Aerospace Engineering; Associate Fellow A.I.A.A.; email: ganguli@aero.iisc.ernet.in
[3] Assistant Professor, Department of Aerospace Engineering; email: dinesh@aero.iisc.ernet.in
[4] Francois-Xavier Bagnoud Professor, Department of Aerospace Engineering; Fellow A.I.A.A.; email: peretzf@umich.edu

Nomenclature

A = main rotor disk area, πR^2
a_0 = section lift curve slope
C_{d_0} = section zero-lift drag coefficient
C_l = section lift coefficient
C_d = section drag coefficient
C_{P_i} = induced power coefficient
C_{P_o} = profile power coefficient
C_P = net power coefficient
C_T = thrust coefficient
$c(r)$ = blade chord
D = drag force on each blade
d_1, d_2 = constants in expression for C_d
$F(r)$ = Prandtl's tip-loss function
FM = figure of merit
L = lift force on each blade
N = number of blade elements
N_b = number of blades
P_i = main rotor induced power
P_o = main rotor profile power
P = main rotor power, $P = P_i + P_o$
R = main rotor blade radius
Re = Reynold's number
r = non-dimensional radial distance
S/N = signal-to-noise ratio
T = main rotor thrust
T/A = rotor disk loading
U = resultant velocity at blade element
BEMT = blade element momentum theory
BET = blade element theory
MAV = micro aerial vehicle
MSD = mean square deviation
OA = orthogonal array
UAV = unmanned aerial vehicle
$\alpha(r)$ = angle of attack
$\theta(r)$ = blade pitch angle
θ_0 = blade collective pitch
θ_{tw} = linear blade twist rate
$\lambda(r)$ = rotor inflow ratio
λ_h = induced inflow ratio at hover
ν = induced velocity
ρ = density of air
σ = rotor solidity
$\phi(r)$ = inflow angle of attack
Ω = rotor angular speed
$(\cdot)_n$ = value of $(\cdot)$ at the mid-point of the n^{th} blade-element

I. Introduction

Interest in development of unmanned aerial vehicles (UAVs) has been increasing continuously. Developed initially for military purposes, UAVs are used for civilian purposes as well. UAVs can be broadly classified, based on the mechanism of lift generation, as fixed wing UAVs, rotary wing

UAVs, and flapping wing UAVs. This paper focuses on rotary wing UAVs.

Rotary wing UAVs, or unmanned rotorcraft, use rotating blades to generate thrust and propulsive forces. They are classified, on the basis of their size and characteristics, as Type-I, Type-II and Type-III unmanned rotorcraft [1].

Type-I unmanned rotorcraft are relatively large in size. Their rotor span is in the range of three to four meters. They are powered by internal combustion engines and therefore have more power. This makes them suitable for autonomous or remotely controlled unmanned rotorcraft missions that require longer endurance (about 30 minutes to a couple of hours) and heavier payload (about 20 to 30 kg or more). Type-I unmanned rotorcraft are dominated by the traditional main-rotor–tail-rotor helicopter configuration having two, three or four main-rotor blades. These unmanned helicopters are typically made of composite materials, aluminium and stainless steel.

Type-II unmanned rotorcraft are smaller in size than their Type-I counterparts. Their rotor span is in the range of one to two meters. They are usually powered by on-board batteries. Most of the remote controlled helicopters used for recreational and hobby purposes fall under Type-II category. These are made of carbon fiber composites and plastics. Type-II unmanned rotorcraft have limited endurance and payload carrying capacity because of their size and power source.

Type-III are the smallest of the unmanned rotorcraft. They are almost entirely made of plastics and are powered by small batteries. Small remote controlled single and multiple rotor helicopters, coaxial rotor helicopters, most of the quadcopters, etc. come under this category. Their small size and light weight makes them attractive for applications involving remote surveillance and stealth monitoring but at the same time makes them unsuitable for applications that require long flight time or large payload carrying capacity.

It is clear that Type-I unmanned helicopters are attractive for practical applications involving unmanned rotorcraft that require significant payload carrying capability and longer endurance. In addition to some of the tasks that can be performed by fixed-wing UAVs, these unmanned helicopters can use their unique abilities such as hover, vertical flight, and slow speed flight in forward, backward and other directions, to perform tasks in a variety of situations. This versatility of unmanned rotorcraft makes them suitable for both military and civilian applications. The MQ-8B Fire Scout developed by Northrop Grumman is used for naval reconnaissance [2]. Yamaha's R-50 and R-MAX unmanned helicopters are used for spraying agrochemicals over farms and for investigative observation of vegetation. The R-MAX has also been used for monitoring volcanic activity, surveying of areas affected by earthquake, monitoring radiation levels during nuclear emergencies, and for detecting damage in bridges and highways [3]. A similar Korean unmanned helicopter called X-Copter is being developed by Oneseen Skytech is intended for agricultural and industrial applications [4]. The Sky Surveyor, an unmanned helicopter developed at Chiba University, is being used to inspect power transmission lines [5]. The use of such unmanned helicopters can also be extended to many other civilian applications such as aerial surveillance in urban areas, traffic monitoring,

broadcasting sports events, aiding and assisting workers and engineers at construction sites, etc.

The huge potential for unmanned helicopters exists since they are suitable for a host of practical applications. Despite their potential, the use of unmanned helicopters in civilian applications has been limited, due to the high costs associated with the development and operation of such unmanned helicopters for civilian applications [4].

The development and operation of unmanned helicopters for civilian applications differs from that for the military applications. For military applications, the unmanned helicopter is expected to operate satisfactorily even in extreme conditions. This requires usage of cutting-edge technologies and high precision components which results in a high cost. For civilian applications, it is sufficient to ensure good performance while keeping the costs low. From an operational standpoint military unmanned helicopters require good performance in all aspects of their flight including hover, axial flight, high rates of climb and descent, and good forward flight performance and maneuverability. However, for many civilian applications, including those mentioned above, the unmanned helicopters are required to operate mostly in the hover condition. Thus, improving the hover efficiency of the unmanned helicopters will significantly reduce their operating costs through improved fuel efficiency, increase the payload carrying capability, and/or increase the flight endurance.

Designing helicopters for improved hover performance alone may affect their performance in forward flight as well. Since the civilian unmanned helicopters need to operate mostly in hover condition or at low speed forward flight, designing them for improved hover efficiency will lead to better overall performance for the entire flight envelope.

A considerable amount of research on hover performance and design optimization of full scale rotorcraft has been conducted [6–8]. However, the results from research on full-scale helicopters are not directly applicable to the small-scale helicopters due to aeroelastic scaling effects [9]. For example, the tip-chord Reynolds number for a typical unmanned helicopter of Type-I category is just under 10^6, which is at least one order of magnitude lower than that of full scale helicopters.

At the other end of the size spectrum, research on rotary wing micro air vehicles (MAVs) has focussed on their design, analysis and hover performance [10]; aeroelastic rotor simulation, design and fabrication [11]; unconventional MAV configurations [12]; and airfoil design for ultra-low Reynolds number flight [13]. While the focus of these studies was on hover performance, design and analysis, and airfoil design for rotary wing MAVs, the Reynolds number regime encountered by these vehicles, which is less than 10000, is well below the Reynolds number encountered by Type-I unmanned helicopters. Moreover, due to their small size these rotary wing MAVs can be classified as Type-III unmanned rotorcraft and therefore have different characteristics compared to the Type-I unmanned helicopters.

There is a surprising lack of available literature on design and analysis of unmanned helicopters that are suitable for many practical civilian applications discussed above. Most of the research on unmanned rotorcraft in this category has focussed on their autonomous navigation and control

aspects.

The main rotor is the most important component of a helicopter. Good main rotor design is critical for ensuring satisfactory performance. The current study considers multiple design parameters of the main rotor of a typical Type-I unmanned helicopter to obtain a robust design using the Taguchi method.

The Taguchi method developed by Dr. Genichi Taguchi in 1956 to improve the quality of manufactured products, is now used in many different engineering fields for robust system design. It is a fractional factorial design of experiments approach, which uses orthogonal arrays of design parameters to reduce the variation in a certain quality characteristic while determining the combination of design parameter values that will lead to enhanced performance. It involves the use of noise values to account for variations in the design parameter values. The use of orthogonal arrays in Taguchi method of design provides a systematic approach for reducing the number of experiments or numerical simulations required for the analysis, and at same time provides an opportunity to independently evaluate the effect of each design parameter on the design.

The usefulness of the Taguchi method has been demonstrated by using it to determine engineering solutions to problems for a variety of applications, including rotor blade design problems. Hu and Rao [14] have used the Taguchi method and it's extensions for developing a robust design methodology for optimizing the power generated by horizontal axis wind turbines. They considered multiple design parameters including chord length at blade root, twist angles at four locations along the blade, number of blades, rotational speed, pitch angle, rotor radius, and hub radius, with the objective of maximizing the power output of the turbine. They have also used the Taguchi method to determine an appropriate set of tolerance settings for the design parameters so as to ensure minimal variability in performance of the turbine. The traditional Taguchi method was extended by them to incorporate behavior constraints such as minimum requirement of power coefficient and maximum limit on induced stress. Mallick et al. [15] have used Taguchi orthogonal arrays for robust design of trailing edge flaps for helicopter vibration reduction. They considered chord length and span of the trailing edge flaps as design parameters with the objective of simultaneously minimizing both helicopter hub vibrations and the flap actuation power, by generating response surfaces from the experimental design points obtained from Taguchi orthogonal array. Bhadra and Ganguli [16] have used Taguchi orthogonal arrays for aeroelastic optimization of helicopter rotor. They considered flap, lag and torsional bending stiffness of the rotor blade as design parameters to simultaneously minimize vibratory hub loads, together with rotor blade root loads in a helicopter, using Taguchi orthogonal arrays to generate the experimental design space. Other applications of the Taguchi to solve a variety of engineering in other fields are given in Ref. [14] and the references therein.

In the current study the Taguchi method is used to obtain a robust design of a small-scale 2-bladed unmanned helicopter by considering 4 design parameters of the main rotor: blade length, blade planform variation (i.e. blade taper), span-wise distribution of blade twist and the rotational

speed. The performance of the resulting robust helicopter design is compared with initial design and is found to have better hover efficiency. The baseline helicopter is modeled to simulate the Yamaha R-50. The objective is to reduce the power required in hover while ensuring that the design is robust enough to remain largely insensitive to reasonable variation in design parameter values.

II. Performance Analysis of Helicopter in Hover

The main rotor is a critical component of the helicopter since it governs three important functions - thrust generation in hover and vertical flight, generation of horizontal component needed for forward flight, and production of forces and moments (jointly with the tail rotor) for attitude and position control. Therefore, an accurate estimation of the main rotor performance is essential for a good rotor design. Even for the case of hover performance prediction is not straightforward since the rotor operates in a complex aerodynamic environment. The aerodynamic models used in the analysis can significantly influence the rotor design. The simplest aerodynamic model includes momentum theory, blade element theory (BET) and the combined blade element momentum theory (BEMT), which are treated in detail in [17] and are summarized below.

A. Momentum Theory

In momentum theory, the rotor blades are replaced by an idealized infinitesimally thin permeable circular disk that produces a pressure difference. The disk generates thrust by imparting velocity to the flow below the disk. The flow is assumed to be one dimensional, incompressible and inviscid. The static pressure far above and below the rotor are considered to be equal to atmospheric pressure. With these assumptions, the thrust and ideal power produced by the rotor are [17]:

$$\begin{aligned} T &= 2\rho A\nu^2 \\ P_i &= \frac{T^{3/2}}{2\rho A} \end{aligned} \tag{1}$$

In non-dimensional form, the thrust and ideal power coefficients are:

$$\begin{aligned} C_T &= \frac{T}{\rho A(\Omega R)^2} = 2\lambda_h^2 \\ C_{P_i} &= \frac{P_i}{\rho A(\Omega R)^3} = \frac{C_T^{3/2}}{\sqrt{2}} \end{aligned} \tag{2}$$

The ideal power ignores losses due to blade drag. BET can account for profile drag losses.

B. Blade Element Theory

In BET, each blade section is represented by a two-dimensional airfoil which produces forces and moments. Wake effects are represented by the induced velocity and the aerodynamic interactions between two blade sections are ignored. Considering a small blade element of length dy, at a distance y, from the rotor axis, the incremental lift and drag forces on this blade section can be written as:

$$\begin{aligned} dL &= \frac{1}{2}\rho U^2 c\, C_l dy \\ dD &= \frac{1}{2}\rho U^2 c\, C_d dy \end{aligned} \tag{3}$$

The blade section lift and drag forces can be resolved along directions perpendicular and parallel to the rotor disk plane, also denoted as the hub plane. The component perpendicular to the disk plane contributes to the rotor thrust and the moment about the rotor axis due to components parallel to the disk plane contribute to rotor power. The incremental rotor thrust and power required due to the contributions from the blade sections of all the rotor blades are:

$$\begin{aligned} dT &= N_b(dL\cos\phi - dD\sin\phi) \\ dP &= N_b(dL\sin\phi + dD\cos\phi)\Omega y \end{aligned} \tag{4}$$

Combining Eqs. (3) and (4), yields the incremental thrust and power coefficients in the non-dimensional form:

$$dC_T = \frac{1}{2}\sigma a_0(\theta(r)r^2 - \lambda(r)r)dr \tag{5}$$

$$dC_P = \lambda(r)dC_T + \frac{1}{2}\sigma C_d r^3 dr \tag{6}$$

$$\Rightarrow dC_P = dC_{P_i} + dC_{P_o} \tag{7}$$

The power coefficient represents the cumulative effects of the induced drag and profile power. The total thrust and power coefficients of the rotor are obtained by integrating Eqs. (5) and (6) over the blade span. The radial variation of inflow is required during this calculation. Obtaining an analytical expression for the inflow variation can be complicated. A relatively simple alternative is to use BEMT [17].

C. Combined Blade Element Momentum Theory

The BEMT combines momentum theory and BET. The rotor blades are idealized into a permeable rotor disk. Conservation of mass, momentum and energy equations are applied to a small annulus of the rotor disk, and the incremental thrust and power are calculated using momentum

theory. It is assumed that successive rotor annuli are independent of each other. The elemental thrust and induced power coefficients of the rotor annulus for hover condition, in non-dimensional form, are:

$$dC_T = 4\left(\lambda(r)\right)^2 r dr \tag{8}$$

$$dC_{Pi} = 4\left(\lambda(r)\right)^3 r dr \tag{9}$$

Invoking the principle of equivalence of the lift (which is the principle behind the BEMT) from momentum theory and BET, i.e. equating Eqs. (5) and (8):

$$\frac{1}{2}\sigma a(\theta(r)r^2 - \lambda(r)r)dr = 4\left(\lambda(r)\right)^2 r dr \tag{10}$$

results in a quadratic equation in $\lambda(r)$ where only one of the roots leads to a physical solution [17]. This is given by:

$$\lambda(r) = \frac{\sigma a_0}{16}\left(\sqrt{1 + \frac{32\theta(r)r}{\sigma a_0}} - 1\right) \tag{11}$$

Using Eq. (11), the inflow can be calculated as a function of r for a given blade pitch, twist distribution, planform variation, and airfoil section. With the calculated inflow, the rotor thrust and power can be obtained by integrating Eqs. (8) and (9) over the rotor disk.

D. Effect of Finite Blade Length

At the blade tip, the air from the bottom surface of the blade, which is at higher pressure, moves over the tip to the top surface which is at lower pressure. This results in formation of trailed vortices at the tip of each blade. The tip vortices result in a high local inflow near the blade tips and reduced lift in the blade tip region. This is known as the tip-loss effect. To account for the effects of tip-loss, Prandtl's tip-loss function is used [17]. Prandtl's tip-loss function is given by:

$$F(r) = \frac{2}{\pi}\cos^{-1}\left(e^{-f}\right) \tag{12}$$

where

$$f = \frac{N_b}{2}\left(\frac{1-r}{r\phi}\right) \tag{13}$$

Considering Prandtl's tip-loss function, the inflow, Eq. (11), is modified and given as:

$$\lambda(r) = \frac{\sigma a_0}{16F(r)}\left(\sqrt{1+\frac{32F(r)\theta(r)r}{\sigma a_0}}-1\right) \tag{14}$$

E. Solution Procedure

In this study, BEMT equations are implemented numerically for predicting the hover performance. The main rotor parameters: number of blades, blade length, blade taper, linear blade twist, the airfoil section and the rotor speed are provided as input for a helicopter with a known gross weight. The steps involved in computing the rotor thrust and power are:

1. The blade is discretized uniformly into a series of small elements (totaling N), each of which are of span Δr (non-dimensional length).

2. The rotor collective pitch, θ_0, is calculated for the required thrust coefficient (which in turn is calculated based on gross take-off weight of the helicopter). Starting from an initial value (based on uniform inflow assumption), the collective pitch is updated iteratively [17].
   Initial value of collective pitch:

$$\theta_0^{(0)} = \frac{6C_{T_{req}}}{\sigma a_0} - \frac{3}{4}\theta_{tw} + \frac{3\sqrt{2}}{4}\sqrt{C_{T_{req}}} \tag{15}$$

   The collective pitch is updated until the predicted rotor thrust coefficient, $C_T^{(i)}$, converges to the required thrust coefficient, $C_{T_{req}}$:

$$\theta_0^{(i+1)} = \theta_0^{(i)} + \left[\frac{6\left(C_{T_{req}} - C_T^{(i)}\right)}{\sigma a_0} + \frac{3\sqrt{2}}{4}\left(\sqrt{C_{T_{req}}} - \sqrt{C_T^{(i)}}\right)\right] \tag{16}$$

3. Next, the inflow and Prandtl's tip loss function are calculated iteratively until convergence, using the discretized forms of equations (12) and (14), given below:

$$\lambda_n = \frac{\sigma a_0}{16F_n}\left(\sqrt{1+\frac{32F_n\theta_n r_n}{\sigma a_0}}-1\right) \tag{17}$$

$$F_n = \frac{2}{\pi}\cos^{-1}\left(e^{-f_n}\right) \tag{18}$$

   where f_n is given by

$$f_n = \frac{N_b}{2}\left(\frac{1-r_n}{\lambda_n}\right) \tag{19}$$

4. Once the pitch, θ_n and inflow, λ_n, have been obtained, the rotor thrust coefficient is calculated from:

$$(\Delta C_T)_n = \frac{\sigma a_0}{2}\left(\theta_n r_n^2 - \lambda_n r_n\right)\Delta r \tag{20}$$

$$\Rightarrow C_T = \sum_{n=1}^{N}(\Delta C_T)_n \tag{21}$$

where, $(\Delta C_T)_n$ is the thrust coefficient of the n^{th} element.

5. The induced power coefficient, calculated based on Eq. (9), is given by:

$$(\Delta C_{P_i})_n = \lambda_n(\Delta C_T)_n \tag{22}$$

$$\Rightarrow C_{P_i} = \sum_{n=1}^{N}\left[\lambda_n(\Delta C_T)_n\right] \tag{23}$$

where, $(\Delta C_{P_i})_n$ is the induced power coefficient of the n^{th} element.

6. With the blade pitch and inflow distribution known, the angle of attack, α, of each of the blade elements can be calculated. With this, the rotor profile power coefficient, C_{P_o}, can be calculated from:

$$(\Delta C_{P_o})_n = \frac{\sigma}{2} C_d r_n^3 \Delta r \tag{24}$$

where, $C_d = C_{d_0} + d_1\alpha + d_2\alpha^2$.

$$\Rightarrow C_{P_o} = \sum_{n=1}^{N}(\Delta C_{P_o})_n \tag{25}$$

7. The net power coefficient of the rotor, C_P, the total rotor power, P, and the rotor figure of merit, FM are calculated from:

$$C_P = C_{P_i} + C_{P_o} \tag{26}$$

$$P = \rho A\left(\Omega r\right)^3 C_P \tag{27}$$

$$FM = \frac{C_T^{3/2}}{C_P} \tag{28}$$

III. Taguchi Method of Design

The Taguchi method of design is a statistical technique that aims to improve the quality characteristic of a product by focussing on the design variables at the design stage itself. It is a fractional factorial design of experiments approach. In the Taguchi method, quality is reflected as consistent performance of a product close to a target value, and reduction in the variation of performance is seen as quality enhancement. The Taguchi method can be used to determine the combination of design parameters that lead to an optimum or enhanced performance of a system, with minimum variation in it's performance [14]. The Taguchi method of design involves two steps:

1. Selecting the values of design parameters such that an optimal (or improved) performance is obtained, and

2. Making the design robust, in the sense that performance remains insensitive to the influence of uncontrollable factors (noise).

This is accomplished by using orthogonal arrays.

Orthogonal arrays are a unique set of tables developed for designing experiments; they represent the smallest fractional factorials which can be used for experimental designs [18]. Orthogonal arrays allow one to determine independently the effect of each design parameter on the overall performance of the system while carrying out a minimum number of experiments or numerical simulations. The generation of Taguchi orthogonal arrays is explained in detail in [19]. Orthogonal arrays are also used to consider uncontrollable variations in design parameter values, also called noise.

Noise factors are factors that affect the performance of the system but cannot be economically controlled. The effect of noise factors on the response of the system under study is called noise. Noise can be due to both internal and external factors and manifests as variations in design parameter values from the desired values that may arise during manufacturing, finishing process, etc. Influence of environmental and other uncontrollable factors will also lead to noise in design parameters.

The use of orthogonal arrays in the Taguchi method of design is enumerated below:

1. Identification of controllable factors and their levels: Controllable factors are design variables which directly influence the system performance. Factor level refers to the different discrete value of the design variables that are considered for design of experiments.

2. Selection of appropriate orthogonal array for design parameters: An appropriate orthogonal array is selected based on the number of design variables and their levels. Standard orthogonal arrays are typically used in applications. The orthogonal array used for the design variables is called design parameter matrix or inner array.

3. Selection of appropriate orthogonal array for noise values: A suitable orthogonal array is selected to account for noise factors based on the number of design parameters that are influenced by noise factors, and their levels. This orthogonal array is known as the noise matrix

or outer array. There is one noise matrix for each experiment or simulation of the design parameter matrix.

4. Analysis of system performance: The average performance of the system and the associated signal-to-noise ratio (S/N ratio), is obtained for each experiment or simulation in design parameter matrix based on the output from the noise matrices. The values of S/N ratios are used to arrive at a robust design of the system.

Signal-to-noise ratio, S/N, is a variance index. It gives an indication of the variation of the quality characteristic for each experiment or simulation of the design parameter matrix. 'Signal' is defined as "the change in the quality characteristic of the system under investigation in response to a factor introduced in the experimental design" [18]; it is a desired effect, as against noise which is undesired. The S/N ratio gives a measure of the sensitivity of the system performance to design parameters, relative to the sensitivity of the system performance to the noise factors. S/N ratio is defined according to the problem objective. There are three commonly used S/N ratios, based on the definition of mean square deviation used:

1. **Smaller-the-better** definition is used in cases where the objective is to minimize the quality characteristic of the system under study. Examples include minimization of shrinkage of cast products, minimization of defects in manufactured products, minimization of heat generated in an electronic or electrical circuit, minimization of induced stresses in a mechanical system, minimization of vibration in machining systems, etc. The S/N ratio for smaller-the-better quality characteristic is given by [18]:

$$\frac{S}{N} = -10 \log_{10} \left(\frac{1}{k} \left[\sum_{i=1}^{k} (y_i)^2 \right] \right) \tag{29}$$

where y_i is the performance characteristic of the i^{th} trial in the noise matrix, and k is the total number of trials in the noise matrix.

2. **Nominal-the-better** is used when the objective is to make the quality characteristic achieve a value as close as possible to a specified target value. Examples where nominal-the-better is used include manufactured products and mechanical fittings, whose dimensions have to be consistently close to a nominal value; ratios of chemicals or mixtures which constitute as the ingredients in a chemical compound; thickness of material deposition or material removal in processes such as electroplating, etching, etc. The S/N ratio for nominal-the-better quality characteristic is given by [18]:

$$\frac{S}{N} = -10 \log_{10} \left(\frac{1}{k} \left[\sum_{i=1}^{k} (y_i - y_0)^2 \right] \right) \tag{30}$$

where y_0 is the specified target (nominal) value.

3. **Larger-the-better** is used when the objective is to maximize the quality characteristic of the system. Examples are maximizing the life expectancy of a product, maximizing the power output of a power generating system, maximizing the range of an aircraft, etc. The S/N ratio for nominal-the-better quality characteristic is given by [18]:

$$\frac{S}{N} = -10 \log_{10} \left(\frac{1}{k} \left[\sum_{i=1}^{k} \left(\frac{1}{y_i} \right)^2 \right] \right) \tag{31}$$

Irrespective of the definition of S/N ratio, the combination of design parameters for which the S/N ratio is highest, will always correspond to the best performance with least variation in performance under the given noise conditions. Thus, the aim of any experiment or simulation is to determine the highest possible S/N ratio. Higher values of S/N ratios indicate higher signal than noise values, i.e., the system is less sensitive to noise factors and thus, uncontrollable factors will not produce large variation in system performance.

IV. Robust Design of a 2-Bladed Unmanned Helicopter Rotor Using Taguchi Method

The robust design of a 2-bladed unmanned helicopter using Taguchi method is described in the following sections. The objective of the parameter design stage is to determine the values of design parameters that lead to improved hover performance. Noise values are considered for each of the design parameters to ensure robustness of the design. The obtained robust design is compared against the baseline Yamaha R-50 helicopter. Analysis of variation (ANOVA) is conducted based on the information obtained from the orthogonal arrays to determine the relative influence of each design parameter on the system performance. Fig. 1 shows the implementation of Taguchi method in the present study. The objective of the tolerance design stage is to determine the optimal tolerance values for the design parameters that yield reduced variation in design parameter values while keeping the costs associated with tolerances as low as possible.

A. Design Parameters and Noise Factors

Based on the expression for the power required for a hovering helicopter, four main rotor parameters are selected as design variables: blade radius, chord length at blade tip (along with blade taper, these capture the blade planform variation), unit linear twist of the blade, and the rotor speed. Three levels of the design parameters are considered. The chord length at the blade tip is also used for determining the rotor blade shape. At level 1, the blade has constant chord whereas it has a linear taper at levels 2 and 3.

Noise values are introduced for each design parameter to analyze the sensitivity of performance

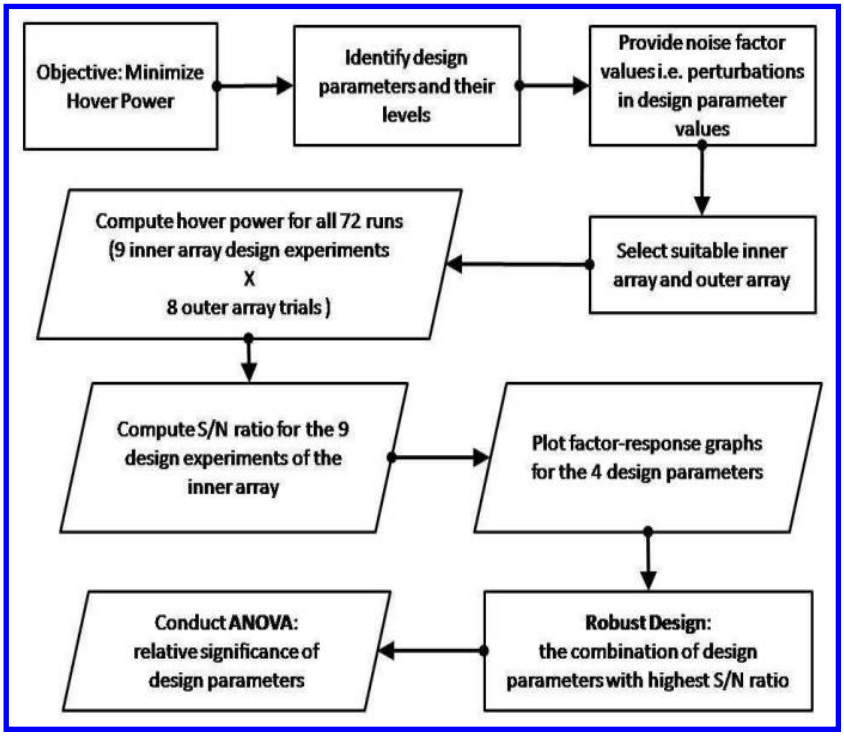

Fig. 1: Flow chart showing implementation of Taguchi method

to noise factors. Following the method used in [14], realistic tolerance of the design parameters have been assumed as noise values.

The values of the design parameters at the three levels along with the noise levels for each design parameter are given in Table (1). The details of the baseline helicopter, Yamaha R-50, are given in Table (2). The airfoil section of the rotor blades, for both the proposed and the baseline design, is assumed to be a NACA 0012 profile.

B. Parameter Design Using Taguchi Method

The parameter design using Taguchi method involves the use of two matrices - the design parameter matrix (inner array) and the noise matrix (outer array). In the present work, 4 design parameters, at 3 levels, are considered. Therefore, the appropriate orthogonal array for design parameter matrix is the standard $L_9(3^4)$ orthogonal array. For the noise matrix, which has 4 variables at 2 levels, the closest standard OA is the standard $L_8(2^7)$ array. The naming convention for OAs is $L_x(y^z)$; where, z represents the number of design parameters being considered, y represents the number of levels of the design parameters, and x represents the number of rows in the OA, i.e. the number of experiments or simulations that are to be carried out.

The standard $L_9(3^4)$ and $L_8(2^7)$ OAs are given in Table (3) and (4), respectively. As can be seen, the $L_8(2^7)$ orthogonal array is best suited for 7 design variables at 2 levels whereas, only 4 noise factors are considered in this work. Therefore, the $L_8(2^7)$ array is not fully populated and the last 3 columns are ignored when constructing the noise matrices. The design parameter matrix and

the noise matrix are obtained by substituting the actual values of the design parameter levels and noise levels in Tables (3) and (4), respectively. For the design parameter matrix, '1' corresponds to least factor level of the design variables, i.e. level 1, and '2' corresponds to the middle factor level, i.e. level 2, and '3' corresponds to the highest factor level, i.e. level 3. The design parameter matrix is given in Table (5).

Each experiment in the design parameter matrix has a corresponding noise matrix. Since, the design parameter matrix has 9 experiments, there will be 9 corresponding noise matrices. Since only four noise factors are considered, only the first four columns of the $L_8(2^4)$ OA are used when constructing the noise matrices. In the present work, tolerance values of design parameters are considered to be noise values. The noise matrix, for each parameter design experiment, is constructed by adding the tolerance values of the design parameters to the corresponding design parameter values. The lower tolerance is used for '1' and the upper tolerance is used for '2', to populate the noise matrix. The 1^{st} experiment of the design parameter matrix is taken as an example to illustrate how the noise matrix is constructed. For the 1^{st} experiment, the design parameter values along with their noise values, (i.e. tolerance), are:

A: Rotor radius $= 1.5 \pm 0.005\ m$

B: Tip chord $= 0.10 \pm 0.005\ m$

C: Blade linear twist $= -5^\circ \pm 1^\circ$

D: Rotor speed $= 800 \pm 5\ rpm$

The noise matrix for the 1^{st} experiment is constructed by adding the tolerance values to the design parameter values, and is shown for a few simulations in Table (6). The hover power required for each simulation is also given in Table (6). The noise matrices for parameter design experiments 2 through 9, along with the power required for each simulation, are given in Tables (7) to (14), respectively.

The values of the power required to hover, obtained from the simulations of the noise matrices, are used to compute the S/N ratios for each parameter design experiment. For each of the 9 parameter design experiments in inner array, 8 simulations are carried out in their corresponding outer arrays. Thus, a total of $(9 \times 8 =)$ 72 simulations are carried out. Since the objective of this study is to minimize the power required to hover, smaller-the-better definition is used to compute the S/N ratios. The robust design with the best hover performance corresponds to the combination of design parameters that yields the highest value of S/N ratio.

The mean power required to hover and the S/N ratios computed for each parameter design experiment are shown in Table (15). From Table (15) it is clear that the 5^{th} experiment of the design parameter matrix corresponds to the highest S/N ratio and also the lowest mean power required to hover. These results indicate that the design parameter setting: A_2, B_2, C_3 and D_1,

yields the robust configuration of the helicopter which has the least power consumption during hover. This robust helicopter configuration, when compared with the baseline helicopter, shows a 11.28% reduction in power required to hover. Table (16) gives a comparison of the baseline helicopter and the robust helicopter design obtained using the Taguchi method.

C. Analysis of variance

Analysis of variance (ANOVA) is carried out, based on the information obtained from the orthogonal arrays, to establish confidence in the robust design methodology adopted. ANOVA involves the use of statistical parameters such as sum of squares, variance, etc. to determine the statistical significance of the design variables considered [18]. The use of S/N ratio in Taguchi method provides a degree of influence that the different design parameter values exert on the performance of the system. Use of ANOVA enables further evaluation of contribution of each design parameter and their relative importance with respect to the performance of the system.

ANOVA calculations are carried out based on the S/N ratios obtained from the 9 numerical experiments. The results are tabulated in Table (17). It is clear from Table (17) that the rotor radius stands out as statistically most significant design parameter with respect to the S/N ratio. The rotor radius is often the first parameter to be fixed in a helicopter, and the other design parameters are obtained subsequently. Thus, the length of the rotor blade is of primary importance. The design parameter ranked 2 is the rotor speed. Rotor speed directly influences the rotor tip speed. The rotor thrust and power vary with square and cubic powers of the rotor speed, respectively. Thus a lower speed is desirable for helicopters for efficient hovering. The blade planform variation is the next most significant design parameter. The ideal planform variation of rotor blades for efficient hover performance is not practically feasible, since it requires a very large root chord. However, a linear taper of the rotor blade planform that is sufficiently close to the ideal taper variation, over most of operational range of the rotor blade, is a good approximation. The taper variation that comes closest to the ideal taper is selected for efficient hover performance. The rotor blade pre-twist has the least statistical significance relative to the other design variables, with respect to the S/N ratio.

D. Tolerance design using Taguchi method

In manufacturing processes, the dimension of each manufactured component varies within a certain small controlled range, called tolerance. The tolerance values are specified for different components based on their functional requirements as well as cost. Components manufactured with smaller/closer tolerance are produced within a narrow range of dimensions, and thus have better quality and reliability. In contrast, large tolerances lead to components that have wider spread in their dimensions leading to fluctuations in their performance and thus poorer quality. However, there is always a conflict between the tolerance and the cost of quality control. Smaller tolerances

require higher costs and hence a small cost may correspond to large tolerances as well as lower quality. As tolerance increases, the cost goes down steeply at the beginning, and then the trend becomes gradually less. Since both quality and cost of the product are important in manufacturing, a combination of these two factors is considered in the tolerance design process. The objective of the tolerance design stage is to reduce the variations in the power required to hover at a reasonable cost, by determining the optimal tolerance values for the design parameters, using the Taguchi method.

In the tolerance design process, each of the design variables used in the parameter design stage is assumed to have three different levels of tolerance as shown in Table (18). The robust design solution achieved in the parameter design stage is used as the mean value for tolerance design. The cost to control the tolerance of the chord length, a linear dimensional, is assumed to be relatively cheap. The twist angle is usually more difficult to control compared to linear dimensions during manufacturing. Thus larger tolerance values are assumed for blade twist per unit length, and the cost of controlling the twist angle is assumed to be two and a half times more than that of linear dimension. The tolerance levels of rotational speed are not too difficult to achieve in practice. Hence, the cost is assumed to be slightly higher than that of controlling a linear dimension. The rotor radius is a large dimension hence, it is assumed to be relatively more expensive than other design variables. The relative costs to control each design parameter considered are summarized in Table (19), and is obtained based on Ref. [14].

Similar to the parameter design stage, the tolerance design using Taguchi method involves the use of two matrices - a design parameter matrix and a noise matrix. The standard $L_9(3^4)$ orthogonal array is used for the design parameter matrix (inner array) and standard $L_8(2^7)$ array (with the last 3 columns neglected) is used for each of the outer arrays. There will be 9 outer arrays with 8 runs in each outer array, which implies that $(9X8 =)$ 72 runs will be carried out in the experiment. The results from the numerical experiments are expressed in terms of S/N ratios. The smaller-the-better definition of S/N ratio, given by equation (29) is used. The quality characteristic used for calculating the S/N ratios is a combination term, the product of fluctuation of power and cost:

$$y_i = \mid \Delta P_i \mid * cost_i \tag{32}$$

where ΔP_i is the difference between actual power and optimum power, and $cost_i$ is the cost of controlling the tolerances of all the design parameters for the i^{th} trial in the outer array.

The results of the 9 simulations of the inner array are summarized in Table (20). According to the smaller-the-better criterion, larger values of S/N ratio correspond to smaller values of the product of power fluctuation and cost. Therefore, the optimal values of tolerances for the design parameters correspond to the 2^{nd} simulation of the inner array. Finally, the optimum solution including both the mean values (optimum values found in parameter design stage) and tolerances (optimum values found in tolerance design stage) can be identified for all the design variables as

shown in Table (21).

V. Conclusion

The present study describes a simple approach for robust design of a small-scale unmanned helicopter for efficient hover performance. Multiple design parameters of the main rotor are considered to obtain a robust design using the Taguchi method. Perturbations are introduced in design parameter values using tolerances, to provide robustness in the design. The performance of the helicopter is predicted using the blade element momentum theory and the analysis is refined using Prandtl's tip-loss function to account for tip-losses. The use of S/N ratios and Taguchi orthogonal arrays results in a systematic reduction in the number of numerical simulations while providing a useful variance index to obtain a robust design solution. The resulting design shows 11.28% reduction in the power required to hover when compared with a baseline helicopter design of similar size and configuration. Considering the overall flight autonomy of such helicopters, this improvement can produce significant gains in terms of operating costs and efficiency. Further evaluation is carried out using ANOVA to determine statistical significance of the design parameters and their relative importance. The Taguchi method is further used in the tolerance design stage to arrive at optimal values of the tolerances for each of the design parameters, that results in reduced fluctuations in hover power values within a reasonable cost of quality control.

References

[1] Cai, G., Chen, B. M., and Lee, T. H., "An Overview on Development of Miniature Unmanned Rotorcraft Systems," *Frontiers of Electrical and Electronic Engineering in China*, Vol. 5, No. 1, 2010, pp. 1–14.

[2] Grumman, N., "MQ-8B Fire Scout," 2011, Accessed on: 19-08-2014.

[3] Sato, A., "The RMAX Helicopter UAV," Tech. rep., DTIC Document, 2003.

[4] Shim, D. H., Han, J.-S., and Yeo, H.-T., "A Development of Unmanned Helicopters for Industrial Applications," *Unmanned Aircraft Systems*, Springer, 2009, pp. 407–421.

[5] Nonami, K., "Prospect and Recent Research & Development for Civil Use Autonomous Unmanned Aircraft as UAV and MAV," *Journal of System Design and Dynamics*, Vol. 1, No. 2, 2007, pp. 120–128.

[6] Walsh, J. L., *Performance Optimization of Helicopter Rotor Blades*, National Aeronautics and Space Administration, Langley Research Center, 1991.

[7] Ganguli, R., "A Survey of Recent Developments in Rotorcraft Design Optimization," *Journal of Aircraft*, Vol. 41, No. 3, 2004, pp. 493–510.

[8] Celi, R., "Recent Applications of Design Optimization to Rotorcraft- A Survey," *Journal of Aircraft*, Vol. 36, No. 1, 1999, pp. 176–189.

[9] Friedmann, P., "Aeroelastic Scaling for Rotary-Wing Aircraft with Applications," *Journal of Fluids and Structures*, Vol. 19, No. 5, 2004, pp. 635–650.

[10] Bohorquez, F., Samuel, P., Sirohi, J., Pines, D., Rudd, L., and Perel, R., "Design, Analysis and Hover Performance of a Rotary Wing Micro Air Vehicle," *Journal of the American Helicopter Society*, Vol. 48, No. 2, 2003, pp. 80–90.

[11] Pounds, P., Mahony, R., and Corke, P., "Small-Scale Aeroelastic Rotor Simulation, Design and Fabrication," *Proceedings of the Australasian Conference on Robotics and Automation*, Citeseer, 2005.

[12] Sirohi, J., Parsons, E., and Chopra, I., "Hover Performance of a Cycloidal Rotor for a Micro Air Vehicle," *Journal of the American Helicopter Society*, Vol. 52, No. 3, 2007, pp. 263–279.

[13] Kunz, P. J., *Aerodynamics and Design for Ultra-Low Reynolds Number Flight*, Ph.D. thesis, Stanford University, 2003.

[14] Hu, Y. and Rao, S. S., "Robust Design of Horizontal Axis Wind Turbines Using Taguchi Method," *Journal of Mechanical Design*, Vol. 133, No. 11, 2011, pp. 111009.

[15] Mallick, R., Ganguli, R., and Bhat, M. S., "Robust Design of Trailing Edge Flap with Orthogonal Array Inspired Response Surface for Helicopter Vibration Reduction," *Proceedings of the 39th European Rotorcraft Forum, Moscow, Russia*, 2013.

[16] Bhadra, S. and Ganguli, R., "Aeroelastic Optimization of a Helicopter Rotor Using Orthogonal Array-Based Metamodels," *AIAA Journal*, Vol. 44, No. 9, 2006, pp. 1941–1951.

[17] Leishman, J. G., *Principles of Helicopter Aerodynamics*, Cambridge University Press, 2nd ed., 2006.

[18] Roy, R. K., *A Primer on the Taguchi Method*, Society of Manufacturing Engineers, 2010.

[19] Kacker, R. N., Lagergren, E. S., and Filliben, J. J., "Taguchi's Orthogonal Arrays are Classical Designs of Experiments," *Journal of Research of the National Institute of Standards and Technology*, Vol. 96, No. 5, 1991, pp. 577–591.

Table 1: Design parameters, levels and noise values

	Design variables	Units	Level-1	Level-2	Level-3	Noise value
A	Rotor radius	m	1.5	1.75	2.0	± 0.005
B	Tip chord	m	0.10	0.08	0.06	± 0.005
C	Blade linear twist	degrees	-5	-7.5	-10	± 1
D	Rotor speed	rpm	800	850	900	± 5

Table 2: Baseline helicopter: Yamaha R-50 [3]

Parameter	Value
Main rotor diameter (m)	3.070
Number of main rotor blades	2
Empty weight (kg) (with fuel)	47
Payload (kg)	20
Overall length (m)	3.580
Overall height (m)	1.080
Overall width (m)	0.700

Table 3: Standard $L_9(3^4)$ orthogonal array

Experiment Number	Parameters A	B	C	D
1	1	1	1	1
2	1	2	2	2
3	1	3	3	3
4	2	1	2	3
5	2	2	3	1
6	2	3	1	2
7	3	1	3	2
8	3	2	1	3
9	3	3	2	1

Table 4: Standard $L_8(2^7)$ orthogonal array

Simulation	Parameters P1	P2	P3	P4	P5	P6	P7
1	1	1	1	1	1	1	1
2	1	1	1	2	2	2	2
3	1	2	2	1	1	2	2
4	1	2	2	2	2	1	1
5	2	1	2	1	2	1	2
6	2	1	2	2	1	2	1
7	2	2	1	1	2	2	1
8	2	2	1	2	1	1	2

Table 5: Design parameter matrix: Inner array $L_9(3^4)$

Experiment Number	Rotor radius A (m)	Tip chord B (m)	Blade linear twist C (degrees)	Rotor speed D (rpm)
1	1.5	0.10	-5	800
2	1.5	0.08	-7.5	850
3	1.5	0.06	-10	900
4	1.75	0.10	-7.5	900
5	1.75	0.08	-10	800
6	1.75	0.06	-5	850
7	2.0	0.10	-10	850
8	2.0	0.08	-5	900
9	2.0	0.06	-7.5	800

Table 6: Noise matrix for 1^{st} experiment: Outer array $L_8(2^4)$

Simulation Number	Rotor radius $R(m)$	Tip chord $c_{tip}(m)$	Blade linear twist $\theta_{tw}(^\circ)$	Rotor speed $\Omega(rpm)$	Hover power P (kW)
1	$(1.5-0.005)$ $=1.495$	$(0.10-0.005)$ $=0.095$	$(-5-1)$ $=-6$	$(800-5)$ $=795$	5.4002
2	1.495	0.095	-6	805	5.4243
3	1.495	0.105	-4	795	5.5420
4	1.495	0.105	-4	805	5.5702
5	$(1.5+0.005)$ $=1.505$	$(0.10-0.005)$ $=0.095$	$(-5+1)$ $=-4$	$(800-5)$ $=795$	5.4493
6	1.505	0.095	-4	805	5.4750
7	1.505	0.105	-6	795	5.4622
8	1.505	0.105	-6	805	5.4908

Table 7: Noise matrix for 2^{nd} experiment

Simulation Number	Rotor radius $R(m)$	Tip chord $c_{tip}(m)$	Blade linear twist $\theta_{tw}(^\circ)$	Rotor speed $\Omega(rpm)$	Hover power P (kW)
1	1.495	0.075	-8.5	845	5.3682
2	1.495	0.075	-8.5	855	5.3928
3	1.495	0.085	-6.5	845	5.5145
4	1.495	0.095	-6	805	5.5432
5	1.505	0.075	-6.5	845	5.4111
6	1.505	0.075	-6.5	855	5.4370
7	1.505	0.085	-8.5	845	5.4464
8	1.505	0.085	-8.5	855	5.4760

Table 8: Noise matrix for 3^{rd} experiment

Simulation Number	Rotor radius $R(m)$	Tip chord $c_{tip}(m)$	Blade linear twist $\theta_{tw}(^\circ)$	Rotor speed $\Omega(rpm)$	Hover power P (kW)
1	1.495	0.055	-11	895	5.3347
2	1.495	0.055	-11	905	5.3595
3	1.495	0.065	-9	895	5.4872
4	1.495	0.065	-9	905	5.5164
5	1.505	0.055	-9	895	5.3703
6	1.505	0.055	-9	905	5.3961
7	1.505	0.065	-11	895	5.4322
8	1.505	0.065	-11	905	5.4627

Table 9: Noise matrix for 4^{th} experiment

Simulation Number	Rotor radius $R(m)$	Tip chord $c_{tip}(m)$	Blade linear twist $\theta_{tw}(^\circ)$	Rotor speed $\Omega(rpm)$	Hover power P (kW)
1	1.745	0.095	-8.5	895	5.8770
2	1.745	0.095	-8.5	905	5.9483
3	1.745	0.105	-6.5	895	6.1474
4	1.745	0.105	-6.5	905	6.2262
5	1.755	0.095	-6.5	895	5.9494
6	1.755	0.095	-6.5	905	6.0219
7	1.755	0.105	-8.5	895	6.1352
8	1.755	0.105	-8.5	905	6.2168

Table 10: Noise matrix for 5^{th} experiment

Simulation Number	Rotor radius $R(m)$	Tip chord $c_{tip}(m)$	Blade linear twist $\theta_{tw}(^\circ)$	Rotor speed $\Omega(rpm)$	Hover power P (kW)
1	1.745	0.075	-11	795	5.0634
2	1.745	0.075	-11	805	5.1114
3	1.745	0.085	-9	795	5.2507
4	1.745	0.085	-9	805	5.3047
5	1.755	0.075	-9	795	5.1065
6	1.755	0.075	-9	805	5.1553
7	1.755	0.085	-11	795	5.2272
8	1.755	0.085	-11	805	5.2835

Table 11: Noise matrix for 6^{th} experiment

Simulation Number	Rotor radius $R(m)$	Tip chord $c_{tip}(m)$	Blade linear twist $\theta_{tw}(^\circ)$	Rotor speed $\Omega(rpm)$	Hover power P (kW)
1	1.745	0.055	-6	845	5.2429
2	1.745	0.055	-6	855	5.2906
3	1.745	0.065	-4	845	5.4901
4	1.745	0.065	-4	855	5.5453
5	1.755	0.055	-4	845	5.3125
6	1.755	0.055	-4	855	5.3619
7	1.755	0.065	-6	845	5.4385
8	1.755	0.065	-6	855	5.4948

Table 12: Noise matrix for 7^{th} experiment

Simulation Number	Rotor radius $R(m)$	Tip chord $c_{tip}(m)$	Blade linear twist $\theta_{tw}(^\circ)$	Rotor speed $\Omega(rpm)$	Hover power P (kW)
1	1.995	0.095	-11	845	6.3514
2	1.995	0.095	-11	855	6.4679
3	1.995	0.105	-9	845	6.6818
4	1.995	0.105	-9	855	6.8082
5	2.005	0.095	-9	845	6.3935
6	2.005	0.095	-9	855	6.5096
7	2.005	0.105	-11	845	6.7537
8	2.005	0.105	-11	855	6.8861

Table 13: Noise matrix for 8^{th} experiment

Simulation Number	Rotor radius $R(m)$	Tip chord $c_{tip}(m)$	Blade linear twist $\theta_{tw}(^\circ)$	Rotor speed $\Omega(rpm)$	Hover power P (kW)
1	1.995	0.075	-6	895	6.5779
2	1.995	0.075	-6	905	6.6900
3	1.995	0.085	-4	895	7.0259
4	1.995	0.085	-4	905	7.1511
5	2.005	0.075	-4	895	6.6839
6	2.005	0.075	-4	905	6.7979
7	2.005	0.085	-6	895	7.0288
8	2.005	0.085	-6	905	7.1573

Table 14: Noise matrix for 9^{th} experiment

Simulation Number	Rotor radius $R(m)$	Tip chord $c_{tip}(m)$	Blade linear twist $\theta_{tw}(^\circ)$	Rotor speed $\Omega(rpm)$	Hover power P (kW)
1	1.995	0.055	−8.5	795	5.2805
2	1.995	0.055	−8.5	805	5.3752
3	1.995	0.065	−6.5	795	5.5871
4	1.995	0.065	−6.5	805	5.6740
5	2.005	0.055	−6.5	795	5.3415
6	2.005	0.055	−6.5	805	5.4192
7	2.005	0.065	−8.5	795	5.5816
8	2.005	0.065	−8.5	805	5.6714

Table 15: Results of 9 parameter design experiments

Experiment No.	Mean Power (kW)	S/N Ratio
1	5.4767	-14.7709
2	5.4487	-14.7262
3	5.4199	-14.6803
4	6.0653	-15.6589
5	5.1878	**-14.3009**
6	5.3971	-14.6448
7	6.6065	-16.4030
8	6.8891	-16.7674
9	5.4891	-14.7931

Table 16: Comparison of baseline helicopter design with robust design

Design parameter	Rotor radius	Tip chord	Root chord	Blade linear twist	Rotor speed	Hover power	Disk loading	Figure of merit
Symbol	R	c_{tip}	c_{root}	θ_{tw}	Ω	P_T	T/A	FM
Units	m	m	m	degrees	rpm	kW	Nm^{-2}	-
Baseline	1.535	0.1044	0.1044	0	850	5.8543	88.79	0.68
Robust	1.75	0.08	0.12	−10	800	5.1857	68.32	0.67

Table 17: ANOVA results for S/N ratios

Parameter	Degree of freedom	Sum of squares	Variance	%Influence	Rank
Blade radius	2	2.8666	1.4333	47.19	1
Tip chord	2	1.2508	0.6254	20.59	3
Blade twist	2	0.1879	0.0940	3.09	4
Rotor speed	2	1.7699	0.8850	29.13	2
Error/Others	0	0	-	0	
Total	8	6.0751		100	

Table 18: Tolerance design: Design parameters and tolerance levels

			Tolerance levels		
	Design variables	Optimum Value	Level-1	Level-2	Level-3
A	Rotor radius	1.75 m	±0.5%	±0.2%	±0.1%
B	Tip chord	0.08 m	±1%	±0.5%	±0.2%
C	Blade linear twist	−10 deg	±20%	±10%	±4%
D	Rotor speed	850 rpm	±10 rpm	±4 rpm	±2 rpm

Table 19: Tolerance design: Design parameters and tolerance levels

		Cost of tolerance at		
	Design variables	Level-1	Level-2	Level-3
A	Rotor radius	666	1500	3000
B	Tip chord	100	200	500
C	Blade linear twist	500	1000	2500
D	Rotor speed	200	300	600

Table 20: Design parameter matrix for tolerance design: Inner array $L_9(3^4)$

Simulation Number	Rotor radius A (%)	Tip chord B (%)	Blade linear twist, C (%)	Rotor speed D (rpm)	Tolerance cost, $	S/N ratio
1	±0.5%	±1%	±20%	±10	1466	−91.1141
2	±0.5%	±0.5%	±10%	±4	2166	−82.9231
3	±0.5%	±0.2%	±4%	±2	4266	−83.5586
4	±0.2%	±1%	±10%	±2	3200	−87.0113
5	±0.2%	±0.5%	±4%	±10	4400	−108.93
6	±0.2%	±0.2%	±20%	±4	2800	−95.0807
7	±0.1%	±1%	±20%	±4	5900	−100.083
8	±0.1%	±0.5%	±4%	±2	4300	−101.734
9	±0.1%	±0.2%	±10%	±10	4700	−111.031

Table 21: Optimal mean and tolerance values of design parameters

Design parameter	Rotor radius	Tip chord	Root chord	Blade linear twist	Rotor speed
Symbol	R	c_{tip}	c_{root}	θ_{tw}	Ω
Units	m	m	m	degrees	rpm
Mean	1.75	0.08	0.12	−10	800
Tolerance	±0.5%	±0.5%	±0.5%	±10%	±4